crystals

MDPI

Article

Effect of Al-Cu-Fe Quasicrystal Particles on the Reinforcement of a Polymer–Matrix Composite: From Surface to Mechanical Properties

Monika Kušter [1,2,*], Zoran Samardžija [1], Matej Komelj [1], Miroslav Huskić [3], Marko Bek [4], Gaël Pierson [5], Richard Kouitat-Njiwa [5], Jean-Marie Dubois [1,2] and Sašo Šturm [1,2,6,*]

[1] Jožef Stefan Institute, Department for Nanostructured Materials, Jamova cesta 39, 1000 Ljubljana, Slovenia; zoran.samardzija@ijs.si (Z.S.)
[2] International Postgraduate School Jožef Stefan, Jamova cesta 39, 1000 Ljubljana, Slovenia
[3] Faculty of Polymer Technology, Slovenj Gradec, Ozare 19, 2380 Slovenj Gradec, Slovenia; miroslav.huskic@ftpo.eu
[4] Department of Industrial and Material Science, Chalmers University of Technology, Rännvägen 2A, SE-412 96 Gothenburg, Sweden; marko.bek@chalmers.se
[5] Institut Jean Lamour, Université de Lorraine, 2 allée André Guinier, 54011 Nancy, France; richard.kouitat@univ-lorraine.fr (R.K.-N.)
[6] Department of Geology, Faculty of Natural Sciences and Engineering, University of Ljubljana, Aškerčeva Cesta 12, 1000 Ljubljana, Slovenia
* Correspondence: monika.kuster@ijs.si (M.K.); saso.sturm@ijs.si (S.Š.)

Abstract: We examined the effect of $Al_{59}Cu_{25}Fe_{13}B_3$ (at.%) quasicrystalline (QC) reinforcement particles on the mechanical and surface properties of a polymer-matrix composite by applying a technical polymer polyphthalamide (PPA). The observed increase in the tensile Young's modulus ranged from 1810 MPa for the pure polymer to 4114 MPa for the composite with a QC filling of 35 vol.%. The elongation at fracture decreased with the filling fraction, being equal to 16.9% for a pure polymer and dropping to 4.8% for the composite with a QC filling of 35 vol.%. The same trend was noticeable with flexural Young's modulus, which ranged from 100 MPa for a pure polymer to 125.5 MPa for the composite with 35 vol.% of QC. It was found that the increase in the mechanical strength led to a simultaneous increase of brittleness, which was reflected in a decrease of the impact strength for a pure polymer from 98.5 kJ/m^2 to 42.4 kJ/m^2 for composites with a QC filling of 35 vol.%. In contrast, when filled with 5 vol.% of QC, the impact strength increased by 8%. The friction coefficient against 100C6 steel dropped from 0.15 for pure PPA down to 0.10 for 5 vol.% of the QC filling, followed by an increase to 0.26 for further QC fillings up to 35 vol.%. Interestingly, a local minimum of friction was achieved at filling factors between 5 to 20 vol.% of QC. Independently, a clear *surfenergy* minimum was also found for the composite material with 20 vol.% of QC filling associated with a net drop in the polar component of the *surfenergy*. *Surfenergy* refers to the surface energy related to the top of the oxide layer under ambient conditions. We hypothesise that this is related to the percolation threshold at about 13 vol.% QC, reflected in the observed behaviour of both the friction coefficient and *surfenergy*. For the pure QC annealed in air for 1 h at 500 °C significant wear tracks were observed accompanied by a wear debris formation. On the other hand, a pure polymer exhibited slightly visible wear tracks with no apparent debris formation, and for the composites with different QC filling factors, the wear traces were barely visible with negligible debris formation.

Keywords: quasicrystals; composite materials; contact angle; surface energy; mechanical tests; friction; wear

Citation: Kušter, M.; Samardžija, Z.; Komelj, M.; Huskić, M.; Bek, M.; Pierson, G.; Kouitat-Njiwa, R.; Dubois, J.-M.; Šturm, S. Effect of Al-Cu-Fe Quasicrystal Particles on the Reinforcement of a Polymer–Matrix Composite: From Surface to Mechanical Properties. *Crystals* **2024**, *14*, 216. https://doi.org/10.3390/cryst14030216

Academic Editor: Shouxun Ji

Received: 17 November 2023
Revised: 12 January 2024
Accepted: 16 February 2024
Published: 23 February 2024

1. Introduction

Quasicrystals (QC) have revolutionized our understanding of crystal order since their discovery in 1982–1984 by Shechtman et al. [1]. These alloys represent a new class of a complex metallic alloys materials characterized by non-translationally-repeating, aperiodic patterns that exhibit a form of order not found in traditional crystals. Unlike regular crystals, quasicrystals display symmetries that were once thought to be impossible in crystal structures, such as five-fold rotational symmetry [2]. Such an atom arrangement naturally results in the creation of a profound pseudo-gap at the Fermi energy. On one hand, there are extended electronic wave functions capable of generating the pseudogap through the diffraction and interference processes with quasiperiodically-stacked atomic planes. On the other hand, there are localized electronic states arising from resonant effects involving nested atomic clusters with self-similar geometries at different. The unique physical properties observed are a direct result of the interplay between the distinct electronic and crystal structures. For instance, of the Al-Cu-Fe alloy the icosahedral (i-phase) exhibits a hardness range of 800–1000 HV. Additionally, it is distinguished by a low friction coefficient, ranging from 0.05 to 0.2, accompanied by excellent wear resistance and reduced adhesion. A comparison of the hardness of pure aluminium, which typically ranges from 25 to 45 HV, and the friction coefficient of aluminium alloys of about 0.37 reveals a superior performance of the QC alloy [3–5]. QCs already found their way into various technological applications in the form of coatings and thin films [6–8] or as reinforcement particles in metal matrices [9]. Quasicrystals used as reinforcement precipitates in maraging steel are used for razor blades, surgical tools or dental wires [9]. A close collaboration between Philips and Sandvik led to the development of a unique, QC-based, stainless-steel shaving blade marketed by Sandvik Steel in Sweden as the Sandvik Nanoflex™ [10]. QC-precipitation-strengthened steel is ductile, corrosion resistant and resilient to ageing.

Polymers exhibit a huge variety of possible chemical compositions and have relatively low cost, ease of processing, acceptable thermal and environmental resistance and recyclability [11]. A major challenge related to the polymers employed in tribological applications at high speed under heavy loads is that they are limited by a low load-carrying capacity and a short operating lifetime [12].

Nowadays, there is a lot of interest in using polymer composites for tribological applications such as gears, wheels, bearings, seals and high wear- and scratch-resistant flexible risers [13–15]. There are already some examples of tailoring polymer-composites tribological properties by using carbon fillers such as carbon nanotubes (CNTs), carbon fibres (CFs) and graphene. Some carbon fillers, such as CNTs, have drawbacks when it comes to developing CNT-reinforced polymer composites due to their high cost and resistance to dispersion in polymer matrices [16].

Based on our current knowledge of composites, we can design novel materials with enhanced properties for specific applications by combining the main features of the different materials in a given composite.

The primary challenge associated with quasicrystals is related to their brittleness around room temperature [2]. An alternative strategy to address this limitation is by using quasicrystals as reinforcing powder within the polymer matrix, where mechanical, tribological, and thermal properties were improved. Examples are epoxy resin [17–19], polyphenylene sulphide [20] and nylon polymer [21]. The most prominent QC-polymer composite was obtained by using the additive-manufacturing technique of selective laser sintering [21].

We chose a more high-end engineering polymer [22] that has never been studied in the context of QC-reinforcement, to the best of our knowledge. Hence, our work focuses on polyphthalamide (PPA) used as a polymer matrix reinforced with different volume amounts of QC powder and adhesion between the QC-powder particles and the polymer matrix with associated surface and mechanical properties.

In our previous study [23], we established that passivating the surface of QCs alters their surface energy, termed *surfenergy*. It is the surface energy of the oxidised QC's surface,

typically in the range of a few tens of mJ/m^2. This is different from the surface energy of bare, unoxidised metallic alloys, which is usually within the range of several hundred mJ/m^2 or higher [24]. *Surfenergy* is crucial because it affects how these treated QCs bond with polymers, changing the overall strength and flexibility of the composite material. It also influences the wetting behaviour of the composite sample depending on the amount of QCs mixed into the polymer. As we show in the following section, the *surfenergy* of this polymer shows a significant polar contribution that is responsible for adhesion to polar liquids such as water.

In addition, we propose that the percolation effect might be an additional key factor for optimising the mechanical properties of composite materials. Percolation happens when enough isolated QC particles in the polymer matrix come together to form a continuous network. This effect likely occurs at a specific concentration of QCs. Other studies have shown that the physical properties of composite materials can peak or drop sharply at certain points. These points, where the rate of change is zero, often line up with the percolation threshold [25]. In our study, we examined how the amount of QCs in the polymer matrix affects friction. We systematically studied the relationship between friction and the concentration of QCs. In this research, we verified this hypothesis through a systematic study of the relationship between friction and the concentration of QCs in the polymer matrix.

This aspect, particularly relevant for refining the surface and mechanical properties of QC-polymer composites, has been overlooked in prior research. Our aim was to explore QC particles' behaviour within the polymer matrix and to determine to what extent the constituting species take part in mechanical and surface properties. Our conclusions are based on characterising the sample surface and mechanical testing using techniques such as scanning electron microscopy (SEM); powder X-ray diffraction (PXRD); friction coefficient (μ); tensile, bending, and toughness testing correlated with Brinell hardness; and the impact strength.

2. Experimental Details

2.1. Input Materials

For the metal part, the quasicrystalline Al-Cu-Fe icosahedral-rich powders doped with small quantities of boron were produced using a special technology by NANOCOM LLC, Moscow, Russia. It is known that small additions of boron, in the range of a few at.% to an Al-Cu-Fe alloy, modify solidification kinetics, favouring the formation of the QC primary phase and lowering the chemical segregation in the cast boron-containing alloy [26].

We characterised the powder as supplied by the producer without any additional information due to special confidentiality relating to the production protocol. The characterisation revealed that the powder was crushed from a master ingot and that it was mechanically sieved. The powder we received was stored in a glove box under argon. The powder was chosen based on several factors, including its potential low cost, low toxicity and availability. For brevity, we label this powder as QC in the subsequent text. Since commercial QC powders contain different phases and there is no corresponding crystallographic database of quasicrystalline phases, as a reference specimen, we employed an already well-studied QC sample. This high-purity reference sample, with a nominal composition of $Al_{59}Cu_{25}Fe_{13}B_3$ (at.%) and a known PXRD, purchased from the Saint Gobain Company, Courbevoie, France (labelled from here as *reference sample*), was sintered from gas atomised powder in a flow of argon using a uniaxial sintering furnace operated at 930 °C and a pressure of 100 MPa [9]. This sample contained a majority of the $Al_{62}Cu_{25}Fe_{13}$ icosahedral quasicrystal phase (i-phase), with no apparent grain texturing and the average grain size of the matrix QC phase being 20–70 micrometres. Additionally, the sample contained small amounts of minor phases, less than 4%, such as $AlFe_2B_2$ and β-AlCu(Fe) and borides AlB_{12} [23].

The polyphthalamide granules (Amodel AT-1002 HS SOLVAY), provided by ALBIS Plastic Vertriebsgesellschaft GmbH, Vienna, Austria, were chosen as the polymer matrix.

Because it is a technical polymer that is used in a wide variety of applications, especially in the automotive industry, and because it can stand relatively high temperatures, it is suitable as a polymer matrix to be reinforced with metal particles. This material is labelled PPA in the subsequent text.

2.2. Composite Fabrication

The desired amounts of polymer and quasicrystal powders were weighed and mixed using a forming process based on a co-rotating twin-screw extruder with a diameter of 20 mm and a length-to-diameter (L/D) ratio of 44 (LABTECH—LTE 20–44, Labtech Engineering Company, Ltd., Bangkok, Thailand). The process extruded the material through a die or nozzle to produce a long filament, which was additionally cut to form the specific shape of the granules. The volume fraction of QC in the composite materials ranged from 0 vol.% to 35 vol.%. Converting mass to volume involves dividing the total mass by the density to yield the volume. The density of dry PPA0 was 1.13 g/cm^3, and for QC powder it was around 4.56 $\pm$ 0.03 g/cm^3. The maximum billet temperature for the extrusion process was set to 335 °C. The final product was in the form of 1.5–2.0-mm granules in the amount of 2 kg. Furthermore, an injection-moulding machine (Arburg, Allrounder 320 C500-100 golden edition, Lossburg, Germany) was used to prepare specimens in the standard dog-bone shape, suitable for characterisation of mechanical properties by tensile, flexural and toughness tests. The melting temperature for injection moulding was fixed at 335 °C, while the mould temperature was lowered to 85 °C, with an injection speed of 40 mm/s, dropping to 10 mm/s for the last 2 mm, after being exposed to a pressure of 550 bars for 10 s, for the net PPA and PPA with 5 vol.% of QCs or 1100 bars for 15 s with a cooling time of 12 s, for the higher fillings with QCs, respectively.

The composites made of a blend of PPA polymer with a volume fraction x of quasicrystal powder (x = 0 vol.%, 5 vol.%, 20 vol.%, 30 vol.%, 35 vol.%) will be labelled PPAx in the subsequent text. For instance, PPA5 means a composite containing 5 vol.% of QC blended with 95 vol.% of PPA.

3. Characterisation Techniques

3.1. Microstructure and Crystal Structure

(a) Scanning Electron Microscopy (SEM)

A JEOL JSM-7600F (JEOL, Tokyo, Japan) field-emission-gun SEM equipped with an energy-dispersive X-ray spectrometer (EDXS) (Oxford Instruments Plc, Abingdon, UK) was used to characterise the microstructures and elemental compositions of the prepared samples. The quantitative EDXS analyses were performed using an Oxford Instruments INCA Microanalysis Suite with an X-Max 20 SDD detector (Oxford Instruments Plc, Abingdon, UK). A sample for the SEM/EDXS microstructural characterisation was prepared using standard metallographic procedures for aluminium alloys. The investigation was performed on a quasicrystalline sample to examine the phases and surface morphology. Images were taken from the central area of the sample using secondary-electron imaging (SEI) for topographic contrast and backscattered-electron imaging (BSE) for compositional Z-contrast to reveal phases with different compositions.

(b) X-ray Powder Diffraction (PXRD)

PXRD data were collected with a Malvern Panalytical Empyrean X-ray diffractometer (Malvern Panalytical, Almelo, the Netherlands) using a monochromated X-ray beam produced by a Cu-target tube ($\lambda K\alpha 1$ = 0.15406 nm and $\lambda K\alpha 2$ = 0.15444 nm). The measurements were obtained with Bragg–Brentano geometry by applying a divergence slit of 0.04 rad, in the range 10 ° < 2 Θ < 100 °, using a step size of 0.0131 ° and with a counting time of 1 s per step. The PXRD data were analysed using the HighScore Plus XRD Analysis Software database PDF-4+ 2023 and based on literature relating to quasicrystals [2].

3.2. Mechanical Tests for the Composite Materials

(a) Tensile test

The uniaxial tensile tests were conducted using a Shimadzu, Ag-X plus 10 KN, universal testing machine, Kyoto, Japan at 1 mm/min rates up to an elongation of 0.25% and then with 50 mm/min rates, respectively. The samples were tested according to the Standard ISO 527 on composite materials.

(b) Toughness test

The Charpy impact strength was investigated using an LY-XJJDS apparatus Liyi Environmental technology, Ltd, Dongguan, China at room temperature. The distance between the supports was 60 mm, and the initial energy assigned to the hammer was 5 J. The composite materials were tested according to ISO 179 standards on un-notched samples. The polymer sample, as well as the composite materials, bent, but they did not break during the test.

(c) Brinell Hardness

Brinell hardness measurements were carried out by applying a hardness tester INNOVATEST NEXUS 7500 (INNOVATEST Europe BV, Maastricht, The Netherlands). The tests were carried out with a load of 15.6 kg using a hard steel ball of 2.5 mm diameter.

(d) Bending test

Three-point flexure tests were carried out using Shimadzu, Ag-X plus 10 KN universal testing machine, Kyoto, Japan at a rate of 2 mm/min. Flexure tests were carried out to 7% strain; therefore, no samples were destroyed.

3.3. Surface-Characterisation Techniques

(a) Contact-angle measurements and determination of the surfenergy

We measured the contact angle and the surface energy (referred to as *surfenergy*) of pure PPA polymer and PPA mixed with different amounts of quasicrystalline pow-der. These measurements were carried out using the Theta Lite-Biolin Scientific instrument, (Biolin Scientific, Göteborg, Sweden) following the detailed methods outlined in [23]. The term *surfenergy* is used to describe the surface energy of a material that has a native oxide layer, which naturally forms on a quasicrystal when exposed to air. As a consequence, the surface energy we deal with is that of the oxidised material, not that of the naked quasicrystals. This principle also applies when the quasicrystals are incorporated into a polymer matrix.

(b) Friction test and wear traces

The friction test was implemented on two different machines: a pin-on-disk apparatus from CSM-Instruments, Peseux, Switzerland (now Anton-Paar) and a low-load tribometer (nano-tribometer) from Anton-Paar, Peseux, Switzerland.

The flat samples were prepared using the same procedure as for the *surfenergy* experiments. It is important to remember that the coefficient of friction is not a property of a single material but rather a property of the entire friction set-up, including the indenter and all its experimental parameters (hardness of the pin, roughness of both sliding surfaces, number of passes, etc.) [27]. For the pin-on-disk experiments, the ball (100C6) had a radius of 6 mm. The test was made at a normal load of 2 N. The stopping point was set at 5000 laps. For the nano-tribometer, the ball (100C6/AISI52100) had a radius of 1 mm. The test was made at a normal load of 10 mN. The length of the linear track was 1 mm. The number of cycles was 200. This test was used to assess the wear undergone by the two contacting bodies, which was expressed by the measure of the distance separating the position along the vertical direction of the indenter holder from a reference plane taken as the origin at the beginning of the test before the load was applied.

4. Results

(a) Microstructure and crystal phases of the input materials

The SEM studies investigated the morphologies and chemical compositions of the polymers and quasicrystalline powders. Figure 1a presents the typical shape and size of the B-doped $Al_{62}Cu_{25}Fe_{13}$ QC powder particles with their unique powder morphology, and Figure 1b is a representative SEM-BSE image of the phases present and identified within the QC particle. The corresponding compositions of the phases detected inside the quasicrystalline powder are presented in Table 1. For the quasicrystalline powder, we confirmed the co-existence of the matrix $Al_{62}Cu_{25}Fe_{13}$ (i-phase), the ternary ω-phase $Al_{58}Cu_{30}Fe_{12}$, the binary β-phase AlCu(Fe) and a minority of the binary Θ-$AlFe_3$ phase. This Fe-rich phase was not a part of the powder-stability region, but it appeared as a residue left in the powder batch, which implies that full mixing of the elements was not achieved upon melting. Such a situation is not unusual in the case of an industrial product. The powder's particle size distribution was bimodal with two distinct fractions, ranging from 0.5 µm to 4–5 µm and from 10 µm to a maximum of 50 µm. Figure 1c,d presents the polymer polyphthalamide resin granules with a size of 2 mm × 1 mm, alongside a BSE micrograph showing a cross-sectional view of the polymer.

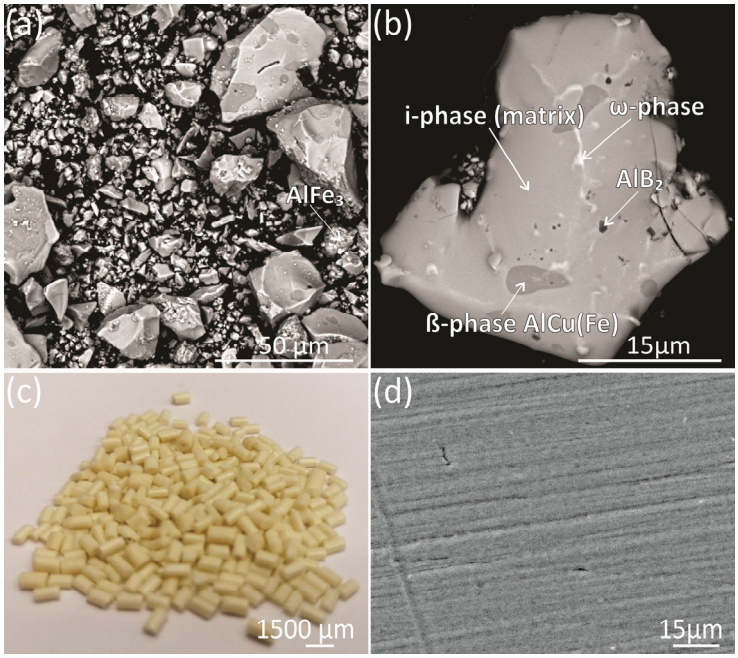

Figure 1. (**a**) Overall SEM-BSE image of the as-received, B-doped $Al_{62}Cu_{25}Fe_{13}$ quasicrystalline powder, (**b**) characteristic higher-magnification BSE micrograph of the detected phases in QC powder. (**c**) Resin granules of the PPA with approximate dimensions 2 mm × 1 mm and (**d**) high-magnification BSE micrograph of the microstructure of the polyphthalamide polymer.

Table 1. Compositions detected by the EDXS with the phases assigned from the PXRD.

Phase Assigned from the PXRD	Detected Composition with EDXS (at.%)	Crystal Structure, Space Group, Number
i-phase $Al_{62}Cu_{25}Fe_{13}$	$Al_{62}Cu_{25}Fe_{13}$	Icosahedral, Fm35
ω-phase	$Al_{58}Cu_{30}Fe_{12}$	Orthorhombic, Immm, 71
β-phase AlCu(Fe)	$Al_{72}Fe_{22}Cu_6$	Cubic, Im-3m, 229
Θ-$AlFe_3$	$Al_{18}Fe_{81}Cu$	Orthorhombic, Bmmm, 65
λ-$Al_{13}Fe_4$	Undetectable by EDXS but confirmed by PXRD	Cubic, Fm-3m, 225
AlB_2	$Al_{28}B_{72}$	Hexagonal, P6/mmm, 191

The PXRD method provided information about the crystallographic structure of the phases in the microstructure of the as-received quasicrystalline powder. The diffraction peaks are indexed using the PDF-4+ 2023 database and the literature relating to quasicrystals [2]. Figure 2 presents the PXRD diffractogram obtained from the as-received QC material based on the $Al_{62}Cu_{25}Fe_{13}$ (at.%) composition, which was used to fabricate the composite materials. Six crystal phases could be confirmed. The major phase corresponds to the quasicrystal icosahedral phase (i-phase, space group Fm35), as verified by a direct correlation of the PXRD pattern obtained from a reference sample with the highest purity of quasicrystalline icosahedral phase [23]. The other minor phases are the cubic β-AlCu(Fe) phase (space group Im-3m, 229), the orthorhombic ω-phase $Al_{60}Cu_{30}Fe_{10}$ phase (space group Immm, 71), the cubic phase λ-$Al_{13}Fe_4$ (space group Fm-3m, 225), orthorhombic phase Θ-$AlFe_3$ (space group Bmmm, 65), and hexagonal phase AlB_2 (space group P6/mmm, 191).

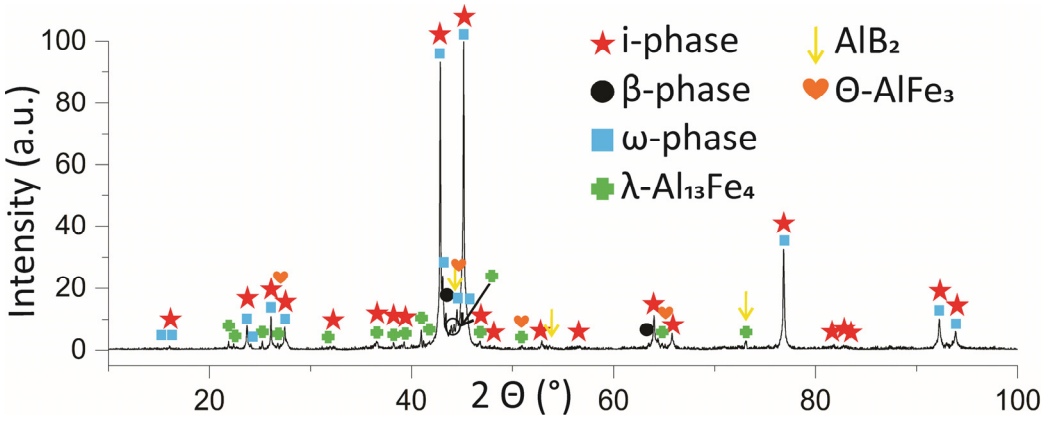

Figure 2. PXRD pattern of the as-received quasicrystalline powder with a nominal composition of $Al_{59}Cu_{25}Fe_{13}B_3$ (at.%). The highest-intensity peaks belong to the $Al_{62}Cu_{25}Fe_{13}$ i-phase. The other minority phases are the β-AlCu(Fe), the ω-$Al_{60}Cu_{30}Fe_{10}$, Θ-$AlFe_3$, λ-$Al_{13}Fe_4$ and boride AlB_2.

(b) Microstructure and structural properties of the composite materials, bonding between the particles and the matrix

Figure 3a presents the overall microstructure of the representative PPA20 fractured surface, Figure 3b presents the overall microstructure of the representative PPA35 fractured surface with visible agglomerates, Figure 3c is a higher-magnification micrograph of the composite PPA5, Figure 3d presents a higher-magnification micrograph of the composite PPA20, Figure 3e presents the overall microstructure of the PPA0 and Figure 3f presents grains of the pure PPA0 after the tensile test, where two different types of plastic deformation are visible.

An analysis of the SEM images of the PPA*x* composites with different volume fillings reveals a nearly homogenous microstructure. No defects and porosity were observed, see Figure 3a,b. Due to the atomic-number (Z) contrast, the Al-Cu-Fe-B particles appear brighter in the SEM–BSE micrographs than in the surrounding carbon-based, low-density PPA matrix. The QC powder particles were distributed uniformly in the polymer matrix. Yet, in composites PPA30 and PPA35, there were occasional cases of particle clustering. Throughout the whole composite, no microbubbles were detected. Figure 3c shows deficient adhesion between the polymer and the QC filler in PPA5, whereas Figure 3d presents good adhesion between the two materials in PPA20; this is visible as the polymer embraces the QC particles. There are no visible pores and voids formed by the ejection of the filler during the mechanical test on the fracture surface.

The PXRD of the composite material was used to verify whether the phases were preserved during the extrusion process when the materials were exposed to temperatures up to 335 °C. Figure 4 shows the PXRD diffractograms of the PPA*x* (x = 0, 5, 20 and 35) composites. The PXRD analysis confirmed the semi-crystalline nature of the polymer,

Figure 4a, which exhibits relatively broader peaks. The XRD spectrums were compared with the XRD pattern of the QC in Figure 2 and the peaks were credibly matched.

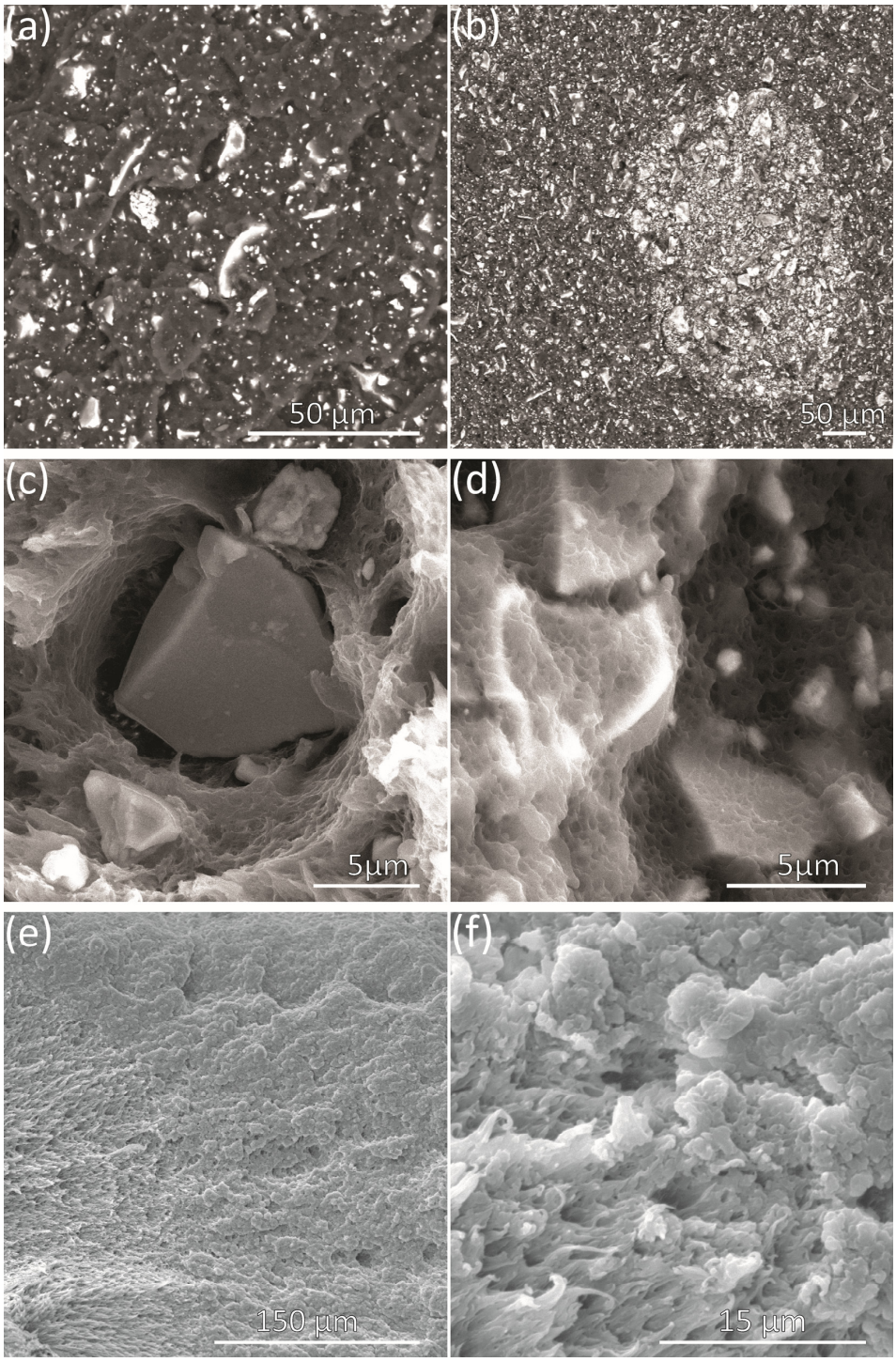

Figure 3. SEM–BSE images of the fracture surface after tensile testing for the composite material with different volumes of filling particles. Overview of the surface morphology after tensile test and fracture of the (**a**) PPA20 and (**b**) PPA35 composite materials, (**c**) characteristic higher-magnification micrograph of the PPA5 composite, (**d**) higher-magnification micrograph of the PPA20 composite, which is also representative for PPA30 and PPA35, (**e**) SEM–SEI image of the fracture surface of the PPA0 polymer after tensile test, and (**f**) characteristic higher-magnification micrograph of the fractured part.

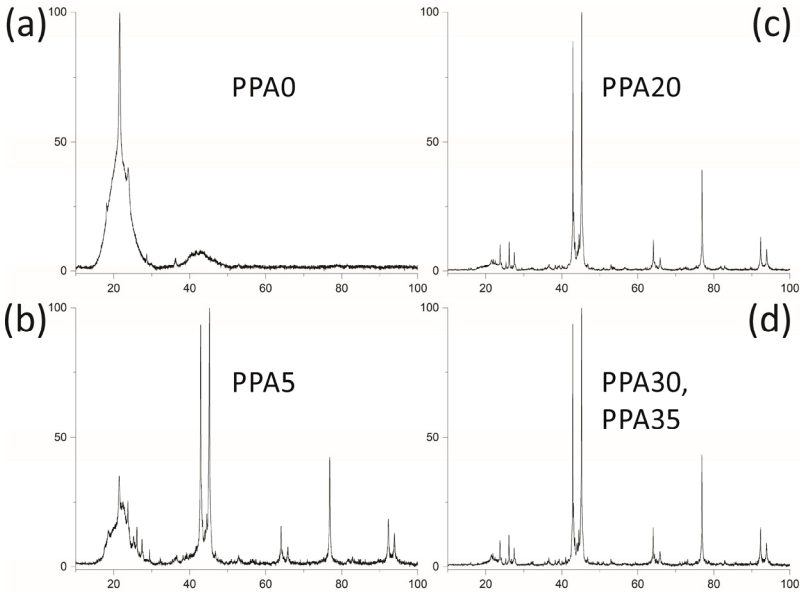

Figure 4. The PXRD patterns for (**a**) the PPA0 pure polymer, (**b**) the PPA5 composite material, (**c**) the PPA20 composite materials, and (**d**) representative diffractogram for both PPA30 and PPA35. The x-axis represents the angle 2 Θ (°), and the y-axis represents the intensity (a.u.).

(c) Mechanical properties of the composite materials

The tensile tests were performed to determine the material's ultimate tensile strength, yield strength, and ductility.

Figure 5 shows the concentration dependency of the tensile Young's modulus and elongation at fracture after tensile tests of the PPA0 and PPAx composites ($5 \leq x \leq 35$ vol.%). The Young's modulus gradually increases from 1810 MPa for the unfilled PPA to 4114 MPa for the PPA35 composite. The elongation at fracture constantly decreases with the filling fraction. It equals 16.9% for an unfilled PPA0, whereas for the PPA35, it drops to 4.8%.

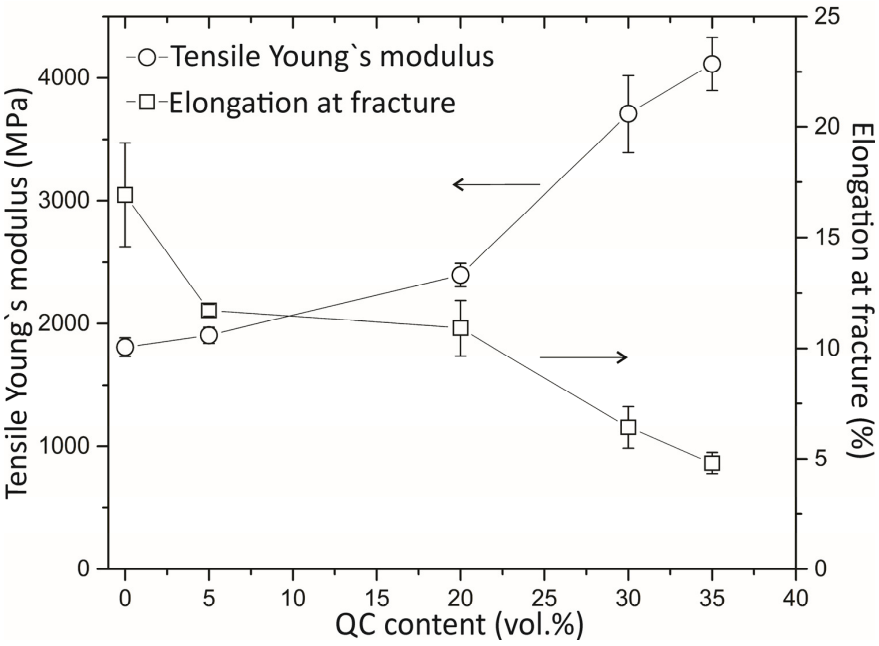

Figure 5. Young's modulus and elongation at fracture of the PPAx ($0 \leq x \leq 35$ vol.%) composites after tensile tests. The arrows specify the axes associated with the results.

Figure 6 presents the flexural strength and the flexural Young's modulus of the PPA0 and PPAx ($5 \leq x \leq 35$ vol.%) composites after three-point flexure tests. An increase of the flexural strength from 100 MPa for PPA0 to 128.5 MPa for composite PPA35 was recorded. The flexural modulus, as in the case of the uniaxial tensile test, increases with increasing the QC content from 20 MPa for PPA0 to 56 MPa for PPA35.

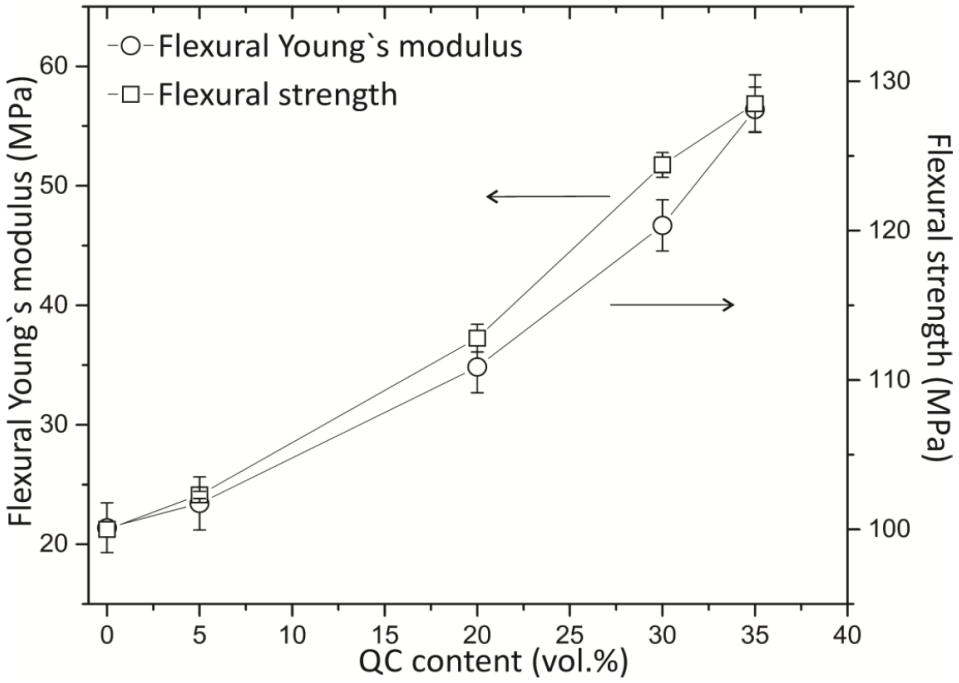

Figure 6. Results of three-point flexure tests for the PPAx ($0 \leq x \leq 35$ vol.%) composites. The arrows specify the axes associated with the results.

Polymers show different levels of brittleness under static and impact loads due to their inherent material properties, including stress-relaxation times. In static load tests, the gradual application of stress allows the material's stress-relaxation processes to play a more significant role, accommodating the applied load over a longer period. In contrast, impact loads apply stress swiftly, providing less time for these relaxation mechanisms to act, which alters the material's response. This distinction in response under different loading rates underscores the importance of impact strength as a key mechanical property in evaluating material properties [27]. Compared to other engineering thermoplastics, PPA stands out for its superior impact strength. It achieves values of 150 J/m [22], which is notably higher than that of nylon, another thermoplastic in the same group, which has an impact strength of only 60 J/m [28].

Figure 7 shows the impact strength of the PPAx ($0 \leq x \leq 35$ vol.%) samples obtained from the Charpy tests applied to our composites with different QC contents. The typical value of the impact strength for PPA0 is 98.5 kJ/m^2, whereas for PPA5, the results show an increased impact strength of up to 107 kJ/m^2. This value decreases to 69.1 kJ/m^2 for PPA20, while it amounts to 50.7 kJ/m^2 for PPA30 and 42.4 kJ/m^2 for PPA35.

The concentration dependence of the Brinell hardness is also shown in Figure 7. The hardness of the PPA0 is 19; no noticeable difference is observed at low filling percentages, but a further increase in the QC content leads to an increase in hardness to 21 for PPA20, 23 for PPA30 and 25 for PPA35.

Figure 8 shows the variation of the coefficient of friction for the PPAx ($0 \leq x \leq 35$ vol.%) composites. The coefficient of friction (μ) changed after adding QC particles, as compared to the pure PPA0, which is equal to $\mu = 0.15 \pm 0.02$. Initially, it decreased at $x = 5$ vol.% and it increased continuously for x above 20 vol.%.

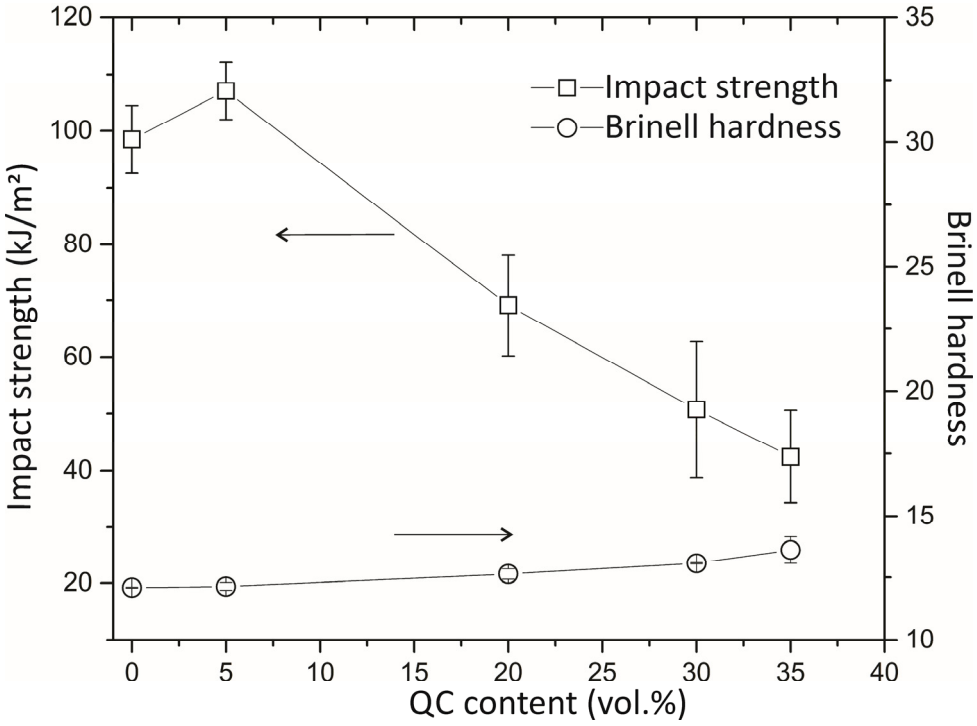

Figure 7. Impact strength and Brinell hardness of the PPAx ($0 \leq x \leq 35$ vol.%) samples. The arrows specify the axes associated with the results.

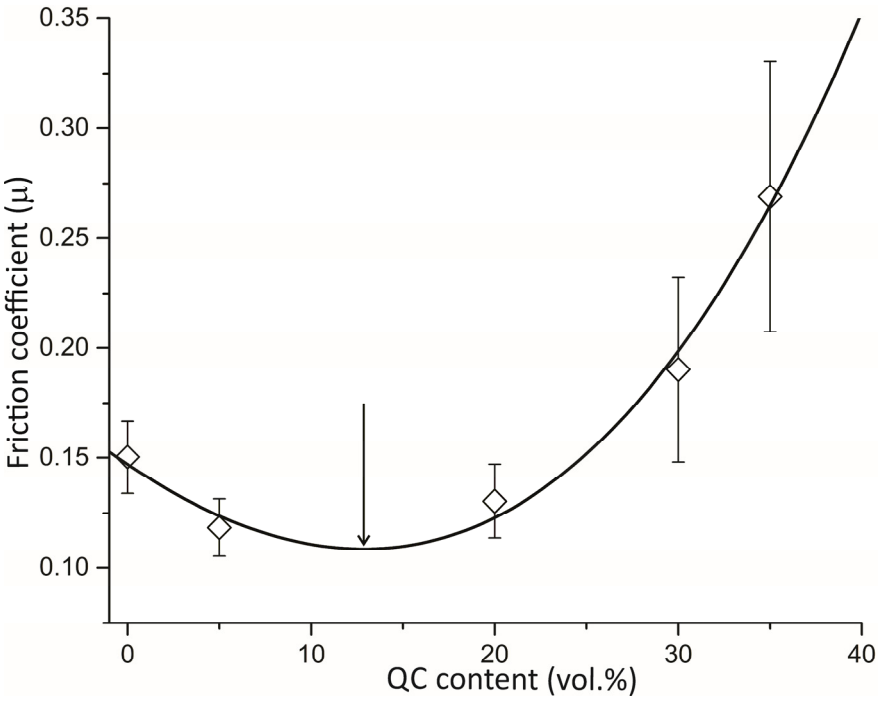

Figure 8. Coefficient of friction measured during pin-on-disk tests performed in air against a hard steel ball on our PPAx (x = 0, 5, 20, 30 and 35 vol.%) composites. The line represents a third-order polynomial fit, which is discussed in Section 4. The arrow marks the minimum of μ, see Section 4.

The SEM investigations of the wear tracks observed on our composites after the pin-on-disk friction test are presented in Figure 9. The *reference* Al-Cu-Fe-B *sample* appeared worn, leaving an exposed trail surrounded by a slightly darkened area that appears to be an Al-rich oxide. A further evaluation of the PPA0 showed a noticeable track compared

to the tracks on the PPA20, PPA30 and PPA35 composites, where the tracks were almost invisible. No additional debris was detected in the wear tracks on the pure polymer and composites, and no oxide layer was found on either.

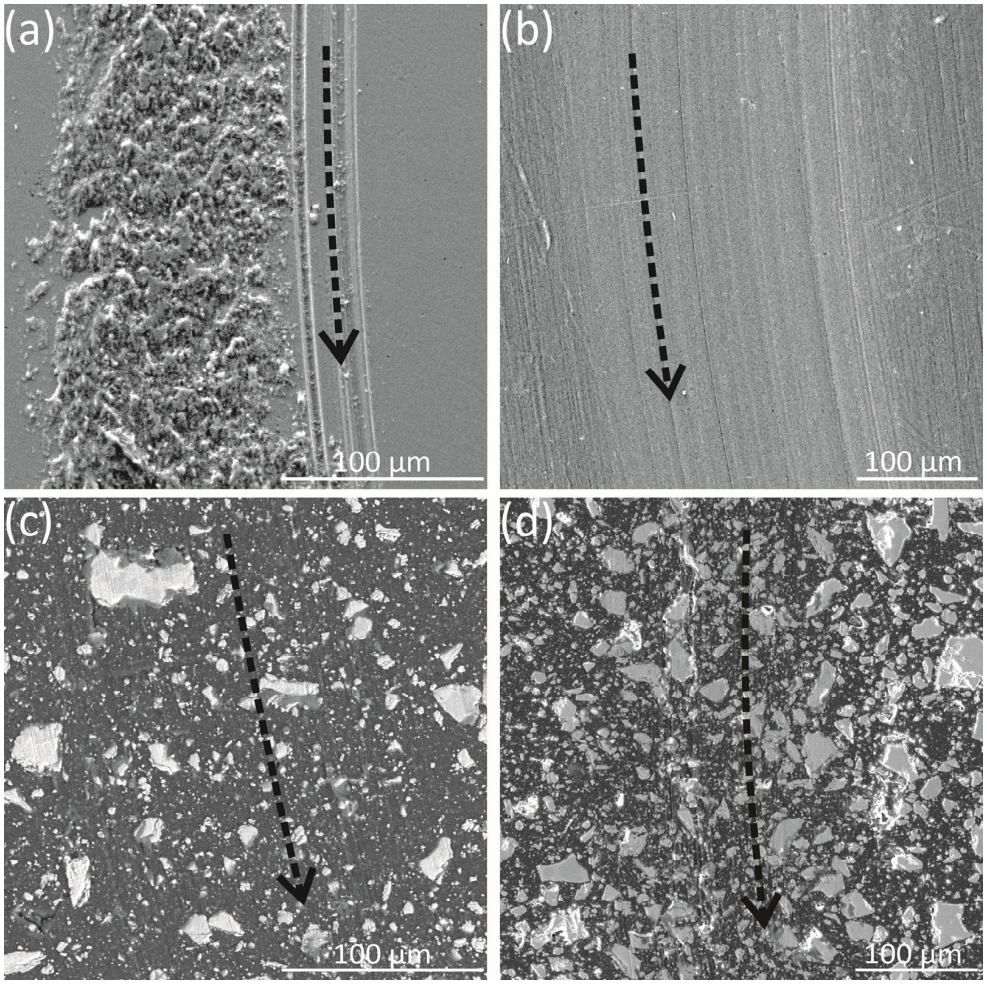

Figure 9. SEM–BSE images of the wear traces (marked by arrows) observed on (**a**) the *reference sample* annealed 1 h for 500 °C in air, (**b**) PPA0, (**c**) PPA20 and (**d**) PPA35. Arrows indicate the path of the wear tracks.

Table 2 presents the output of the contact-angle measurements performed using water and diiodomethane on the composite materials. Figure 10 presents the calculated data of the *surfenergy* and their components on the PPAx ($0 \leq x$ 35 vol.%) composites. It is noticeable that there are almost no visible changes in the dispersive component after adding up to 35 vol.% of the QC particles to the polymer matrix. The dispersive component remained in the range $\gamma_{sv}^{d} = 33 - 34 \pm 1$ mJ/m^2. A slightly different trend is visible for the polar component, which dropped from the initial value of $\gamma_{sv}^{p} = 5 \pm 2$ mJ/m^2 for the PPA0 to $\gamma_{sv}^{p} = 1.2 \pm 0.6$ mJ/m^2 for the PPA20, to $\gamma_{sv}^{p} = 4 \pm 1$ mJ/m^2 for PPA30, and to $\gamma_{sv}^{p} = 3 \pm 0.5$ mJ/m^2 for PPA35. Consequently, the *surfenergy* of the pure PPA0 was equal to $\gamma_s = 39 \pm 2$ mJ/m^2. The total value was not affected for PPA5, which resulted in $\gamma_s = 39 \pm 2$, whereas for PPA20, it resulted in a drop to $\gamma_s = 36 \pm 1$ mJ/m^2. A further measurement for PPA30 or PP35 yielded only a small change to $\gamma_s = 37 \pm 2$ mJ/m^2.

Table 2. Surface characteristics of the pure PPA and composite materials.

Material	Contact Angle Water (°)	Contact Angle Diiodomethane (°)	Dispersive Component γ_{sv}^{d} (mJ/m^2)	Polar Component γ_{sv}^{p} (mJ/m^2)	Surfenergy γ_s (mJ/m^2)
PPA0	77.1 ± 1.1	50.6 ± 0.7	33.9 ± 0.8	4.6 ± 0.9	38.5 ± 1.7
PPA5	78.8 ± 2.5	49.9 ± 0.3	34.3 ± 0.3	3.9 ± 1.7	38.2 ± 2
PPA20	88.0 ± 2.5	49.1 ± 0.6	34.8 ± 0.4	1.2 ± 0.6	36 ± 1
PPA30	79.2 ± 1.8	52.6 ± 0.8	32.8 ± 0.7	4.1 ± 1	36.9 ± 1.7
PPA35	80.5 ± 0.7	50.0 ± 0.4	34.3 ± 0.3	3.3 ± 0.5	37.6 ± 0.8

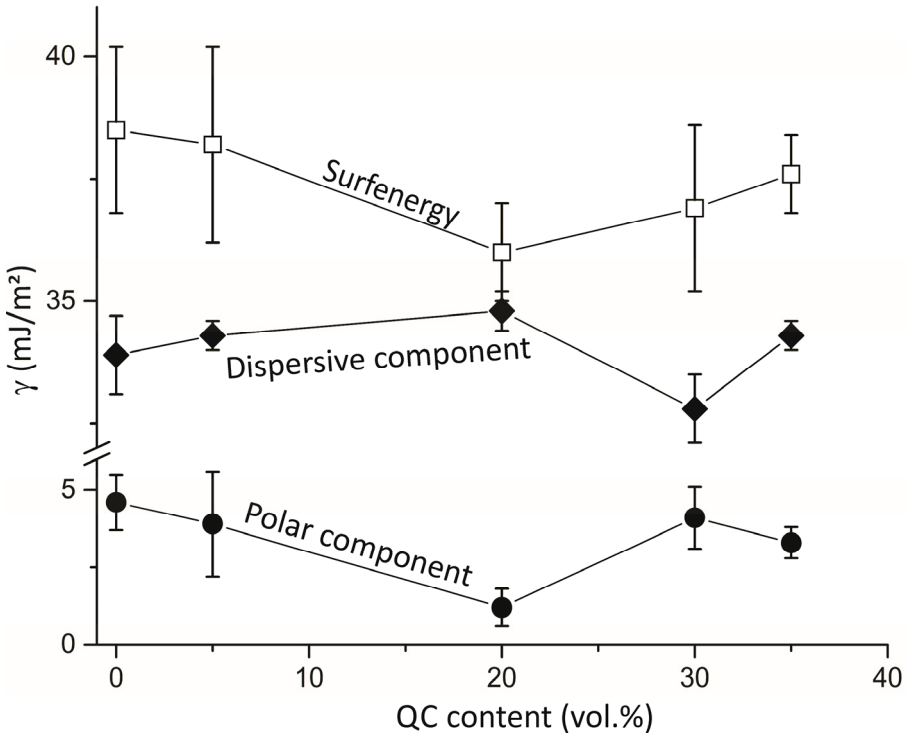

Figure 10. Evolution of the *surfenergy* (open squares), dispersive (solid diamonds) and polar (full circles) components of the PPA*x* composite materials. Symbols are connected by solid lines only as a guide for the eye.

5. Discussion

SEM studies were performed on a fracture surface to understand better the composite materials' microstructure and the bonding between the QC particles and the polymer matrix. Concerning practical use, QC particles may exhibit clumping during storage or extrusion mixing, resulting in a composite product with limited usability. Therefore, concerning the formation and handling of small particles of micro and nano sizes, agglomeration [29] is a challenge [30]. We observed that the QC distribution of the particles within the polymer matrix was homogenous, although some agglomerates embedded in the matrix form in composites PPA30 and PPA35. The same effect of particle distribution and the formation of agglomerates was noticeable when the quasicrystals were embedded in epoxy [17]. They emerged due to a small particle size, which facilitated agglomeration. Another factor contributing to the presence of agglomerates was an enhanced viscosity during extrusion [31] due to an increased volumetric fraction of QC particles, making mixing between the QC and the matrix more difficult. As the extrusion temperature is lower than the necessary sintering temperature, the potential sintering of individual particles into polycrystalline bodies has been eliminated.

A further observation with the SEM was the wetting of the resin in the QC particles. According to Anderson [32] wettability is defined as the fluid's tendency to spread on a surface or to adhere to a solid surface. Despite mixing materials with different properties, which form a weak or even a non-existent interface, the QC particles are essentially completely enveloped by the polymer matrix, as shown in Figure 3c,d. A favourable wetting between the matrix and the reinforcement phase is the initial requirement for the formation of a good interface and consequently for strong forces between the particles and the polymer matrix.

Another phenomenon typical for PPA–QC (polyphthalamide–quasicrystal) composites is a gradual increase in the hardness with the filler content. The observed increase in the hardness of such composite materials is governed by the very high QC hardness, which can reach values of 8–10 GPa in bulk samples [2] and up to 14 GPa in thin films at room temperature, as compared with hardened steel, which does not exceed 8 GPa.

To check whether the extrusion process leads to any degradation of the polymer or to a change in the composition of the initial QC powder, the PXRD was performed on the pure polymer and PPA*x* composites. Indeed, in the PXRD diffractogram of the composite material, there is evidence for a minor phase in addition to the major i-phase in the initial QC powder (Figure 4), which calls for further experiments. On the other hand, the crystallinity of polymers serves as a fingerprint for a polymers' identification, and it offers a qualitative measure of the degree of crystallinity, which defines the optical, mechanical, thermal and chemical properties. After adding the QC particles to the polymer matrix, the nature of the polymer was evidently maintained, regardless of the volumetric amount of QC filling.

We examined wear traces formed during the pin-on-disc experiment, as shown in Figure 9. Pronounced wear tracks were observed on the sintered QC sample, which was accompanied by the formation of a significant amount of debris. The debris formation was attributed to the inherent brittleness of the quasicrystals. Conversely, a polymer characterised by a notable degree of elasticity manifests only visible wear traces, with no debris formation, due to its propensity for plastic deformation. Contrary to expectations assuming the brittleness of quasicrystals, the PPA–QC composite material displays a marked plastic behaviour. This unexpected behaviour underscores the superior mechanical properties of the composite when compared to the individual constituents—pure PPA and QC—and emphasises the advantageous properties achieved through the combination of dissimilar materials in a composite, showcasing the potential for tailoring materials to achieve a balance of mechanical characteristics that surpass the individual components.

The observed increase in Young's modulus with higher QC contents can be attributed to the enhanced fracture toughness, which, on the other hand, is accompanied by a decrease in the plasticity of the PPA–QC composites due to a reduction in the elongation values at the break. The observed trend must be driven by the QC's mechanical properties and the interactions at the PPA–QC interface. However, the dependence of the impact strength, which measures the brittleness, on the QC content is slightly different. While the material PPA5 has a higher impact strength than the pure polymer, this strength decreases with additional QC filler, reaching 42.4 kJ/m^2 for PPA35. This decrease suggests a possible percolation effect.

In the context of the measured coefficient of friction, a distinct pattern emerges with PPA*x* materials. Initially, PPA5 shows a 20% reduction in friction compared to PPA0. This decrease is attributed to the hardness of the QC particles reinforcing the polyphthalamide matrix, which minimises plastic deformation during wear and friction tests. However, as more QC particles are added to the matrix, there is a significant increase in friction. This increase reaches up to 100% for the PPA35 sample, which contains the maximum amount of QC fillings.

As shown in Table 3, QCs, particularly Al-Cu-Fe, exhibit significantly lower friction coefficients compared to alloys of similar hardness (about 7–8 GPa, according to ref. [33]) and Young's modulus (around 100 GPa, as reported in ref. [34]). Notably, in complex

crystals, friction correlates with electronic conductivity, offering insights into the unique anisotropic friction seen in decagonal quasicrystals, as discussed in refs. [2,4]. The low friction coefficient observed suggests that using these materials as binders in polymers could lead to enhanced technological applications compared to traditional hard metals. Furthermore, wear, which is closely related to friction, especially in conventional materials, shows improvement in PPA–QC composites. This improvement in wear performance is mainly due to the QC's hardness and its low friction coefficient. Additionally, literature comparisons (Table 3) suggest that among various composite materials, those combining quasicrystals with the PPA polymer still have the lowest friction coefficients.

Table 3. Friction coefficient of different materials relevant to the present study compared to the literature data.

Material	Against Material	Static Coefficient of Friction (Dry Contact)	Reference
Aluminium	Steel *	0.61	Ref. [35]
Aluminium-Bronze alloy	Steel *	0.46	Ref. [35]
Steel	Steel *	0.8	Ref. [35]
Epoxy	Steel *	0.2–1	Ref. [36]
Nylon (PA)	Steel *	0.15–0.25	Ref. [35]
Quasicrystal with excellent lattice in vacuum	Steel *	0.07	Ref. [2]
Quasicrystal with excellent lattice in the air	Steel *	0.6–0.8	Ref. [2]
Composite (epoxy resin + Al_2O_3)	Aluminium	0.4–0.6	Ref. [37]
Composite Polyamide + QCs	Steel *	0.21	Ref. [21]
Quasicrystal annealed in air 1 h 500 °C	100C6 steel	0.2	this work
Polyphthalamide PPA0	100C6 steel	0.15	this work
PPA5	100C6 steel	0.12	this work
PPA20	100C6 steel	0.13	this work
PPA30	100C6 steel	0.19	this work
PPA35	100C6 steel	0.27	this work

* For the tribology tests 100Cr6 or 100C6 steel is typically used. The given literature does not detail the steel type used in the respective study.

The observed relationship between the impact strength and the coefficient of friction based on the QC content in the polymer suggests a potential percolation effect, as shown in Figure 11.

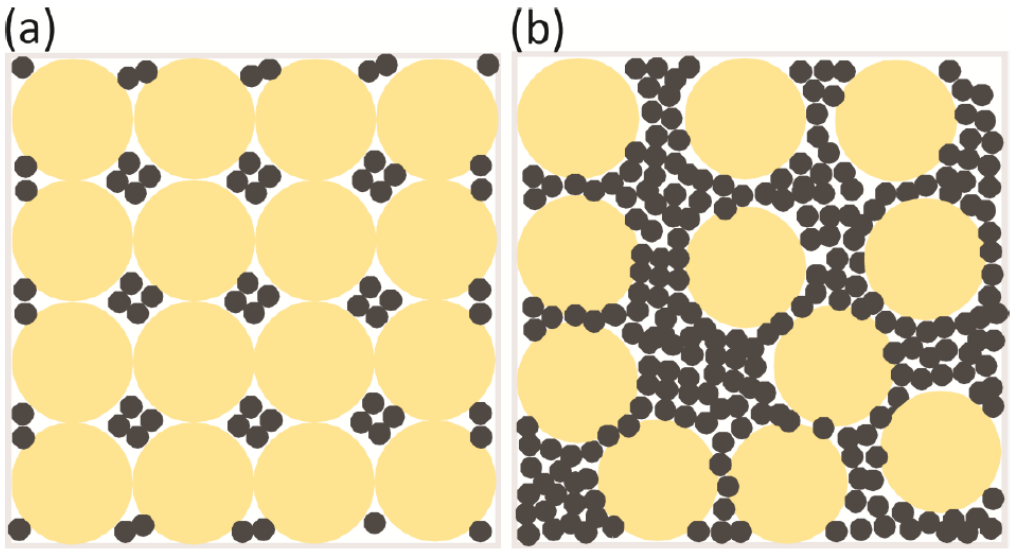

Figure 11. Idealized presentation of the percolation mechanism for (**a**) $x < x_p$ and (**b**) $x > x_p$. To simplify the figure, the QC particles are represented by black circles, whereas their actual shape is not spherical.

The friction increases with the QC content, but the value for a pure polymer is higher than that of a low QC content. A mirrored phenomenon is observed in the case of impact strength. It might be that only non-connected QC particles act as a lubricant, hence lowering the coefficient of friction, whereas the strengthening of the bonds between QC particles during the growth of a network above the percolation threshold has the opposite effect. To quantitatively support the hypothesis, we phenomenologically approximate the coefficient of friction $\mu(x)$ dependence on the QC content x using a third-order polynomial as:

$$(x) = a + bx + cx^2 + dx^3 \quad (1)$$

where a, b, c and d are unknown coefficients that are obtained from the optimum least-squares fit to the experimental data presented in Figure 9, resulting in (a = 146.944, b = −5.545, c = 0.167, and d = 0.003) × 10^{-3}, with x expressed in volume %.

We observe the minimum in the coefficient of friction, defined by the content x derivative of Equation (1) $d\mu/dx$, equals zero. It is seen as the predicted percolation threshold, the content at which a QC continuous network is formed throughout the whole sample (x_p). The derivative:

$$\frac{d}{dx} = x_p = 3dx^2 + 2cx + b \quad (2)$$

set to zero $d\mu/dx = 0$, yields x_p = 13 vol.%. We assign this minimum in the friction to an optimum filling of the PPAx composite with 13 vol.% of QC particles that undergoes a percolation of the powder grains within the polymer granules in the loading chamber of the twin-screw extruder. When the PPAx ($x > 0$) blend is introduced to this chamber and just before the pressure starts to increase, or equivalently when the QC particles are no longer free to move over long distances, the composite state is different, depending on whether the polymer granules form a continuous network ($x < x_p$) or when the polymer granules no longer form a continuous network ($x > x_p$). These two different situations are pictured in Figure 11. Let us assume that the polymer granules are close enough to a spherical shape and are all the same size. When the pressure starts to increase, these spheres form a dense packing, with a packing fraction equal to:

$$\eta = \frac{\pi}{\left(3\sqrt{2}\right)} = 0.74 \quad (3)$$

The remaining volume fraction 1–η can accommodate the QC grains, which pack randomly. Due to their irregular shape, their own packing fraction cannot exceed $\nu = 0.5$ [25]. Consequently, the maximum volume fraction that can be incorporated into the blend of polymer granules before the polymer granules no longer form a continuous network is $(1–\eta)\nu = 0.13$. Therefore, we attribute the observed minimum in the friction and the plateau in other mechanical properties of our PPAx composites to a percolation threshold that occurs around x_p = 13 vol.% during the preparation of the composite blend. Below this threshold, the polymer forms a continuous network, whereas, above this threshold, the powder grains have accumulated in the areas separating the granules. Consequently, the friction increases due to the brittle fracture of the QC-rich areas and debris formation, while the elongation at fracture and the impact strength decrease. Pinning effects become significant in the observed wetting behaviour.

6. Conclusions

In this study, we demonstrated the basic underlying optimisation of composites. The most valuable additional contribution is a demonstration of the link between the *surfenergy*, friction and a percolation threshold of the dual powder filling, resulting in the achievement of the optimum mechanical properties. The investigated composites exhibited a good distribution of QC particles within the polymer matrix up to the fillings of 20 vol.%. The presence of agglomerates was noticeable only for the PPA30 and PPA35. It was shown that the introduction of QC particles in the polymer matrix led to higher values of Young's modulus for the composite materials, as measured by both, the tensile and the three-point flexure tests, accompanied by an increase in the Brinell hardness. The impact strength reached the maximum for the PPA5. A decrease in plasticity was observed for the QC fillings of more than 20 vol.%, at which the material became more brittle. A good wettability of the polyphthalamide matrix around the quasicrystalline particles was achieved and confirmed by means of the SEM imaging of the PPA–QC powder interface. The friction coefficient decreased for PPA5, followed by the continuous increase for filling volumes above 20 vol.% of QC. By determining the *surfenergy*, we estimated the values of the composite's polar and dispersive components. We concluded that the only significant change in the polar component occurred for the composite PPA20. We hypothesise that the percolation threshold at about 13 vol.% QC is reflected in the observed behaviour of the impact strength and the friction coefficient. The presence of the QC powder in the polymer matrix caused a low abrasion of the steel counterpart materials and, consequently, a high wear resistance. A combination of the desired QC and polymer properties, as demonstrated in this study, indicates the investigated materials as technologically promising in applications where it is essential to simultaneously minimise the wear-induced mechanical debris and to preserve excellent mechanical properties such as strength, hardness and toughness of the PPA–QC composite. The PPA–QC composites we developed are highly promising for use in automotive and whiteware appliances, where they intersect mechanical integrity with high strength, low wear, and minimal adhesion. This is particularly beneficial in components like bearings and cogs. They are also promising in mitigating fretting, a tribological issue arising from small oscillatory movements in parts such as space antennas during launch and operation. These findings pave the way for future production of these vital components to avoid system failures.

Author Contributions: Conceptualization, M.K. (Monika Kušter); Methodology, M.K. (Monika Kušter); Validation, M.K. (Monika Kušter), Z.S., M.K. (Matej Komelj), M.H., M.B., R.K.-N., J.-M.D. and S.Š.; Formal analysis, M.K. (Monika Kušter), Z.S., M.K. (Matej Komelj), M.B. and G.P.; Investigation, M.K. (Monika Kušter); Resources, M.K. (Monika Kušter); Data curation, M.K. (Monika Kušter), Z.S., M.K. (Matej Komelj), M.H., M.B., G.P., R.K.-N., J.-M.D. and S.Š.; Writing—original draft, M.K. (Monika Kušter); Writing—review & editing, M.K. (Monika Kušter), Z.S., M.K. (Matej Komelj), M.H., M.B., R.K.-N., J.-M.D. and S.Š.; Visualization, M.K. (Monika Kušter); Supervision, J.-M.D. and S.Š.; Project administration, S.Š.; Funding acquisition, S.Š. All authors have read and agreed to the published version of the manuscript.

Funding: This research received no external funding.

Data Availability Statement: The original contributions presented in the study are included in the article, further inquiries can be directed to the corresponding author.

Acknowledgments: This work was performed within the frame of the IRP PACS2 project. The research was financially supported by Slovenian Research Agency (P2-0084), CNRS and Université de Lorraine, France, and the European Union Horizon 2020 research and innovation programme under grant agreement No. 823717—ESTEEM3. We are grateful to Borut Žužek for generously providing us with the Brinell Hardness tests, and we would like to express our gratitude to Elzbieta Krol for her invaluable assistance during the extrusion process.

Conflicts of Interest: The authors declare no conflict of interest.

References

1. Shechtman, D.; Blech, I.; Gratias, D.; Cahn, J.W. Metallic phase with long-range orientational order and no translational symmetry. *Phys. Rev. Lett.* **1984**, *53*, 1951–1953. [CrossRef]
2. Dubois, J.-M. *Useful Quasicrystals*; World Scientific Publishing Co Pte Ltd.: Singapore, 2005; p. 504.
3. Belin-Ferre, E.; Berger, C.; Quiquandon, M.; Sadoc, A. *Quasicrystals Current Topics*, 1st ed.; World Scientific Publishing Company: Singapore, 2000; p. 544.
4. Maciá-Barber, E. *Quasicrystals Fundamentals and Applications*, 1st ed.; CRC Press, Taylor & Francis Group, LLC: Boca Raton, FL, USA, 2021; p. 388.
5. Rabson, D.A. Toward theories of friction and adhesion on quasicrystals. *Prog. Surf. Sci.* **2012**, *87*, 253–271. [CrossRef]
6. Ledieu, J.; Fournée, V. Surfaces of quasicrystals. *Comptes Rendus Phys.* **2014**, *15*, 48–57. [CrossRef]
7. Jenks, C.J.; Thiel, P.A. Quasicrystals: A Short Review from a Surface Science Perspective. *Langmuir* **2002**, *14*, 1392–1397. [CrossRef]
8. Yadav, T.; Mukhopadhyay, N. Quasicrystal: A low-frictional novel material. *Curr. Opin. Chem. Eng.* **2018**, *19*, 163–169. [CrossRef]
9. Dubois, J.-M. Potential and marketed applications of quasicrystalline alloys at room temperature or above. *Rend. Lincei. Sci. Fis. e Nat.* **2023**, *34*, 689–702. [CrossRef]
10. Nanotechnology Products Database (NPD). *Sandvik Nanoflex Strip Steel Datasheet*; Sandvik Materials Technology: Sandviken, Sweeden, 2018.
11. Mittal, V. (Ed.) *High Performance Polymers and Engineering Plastics*; John Wiley & Sons: Hoboken, NJ, USA, 2011; p. 452.
12. Lin, A.-D.; Kuang, J.-H. Dynamic interaction between contact loads and tooth wear of engaged plastic gear pairs. *Int. J. Mech. Sci.* **2008**, *50*, 205–213. [CrossRef]
13. El-Sayed, A.; El-Sherbiny, M.; Abo-El-Ezz, A.; Aggag, G. Friction and wear properties of polymeric composite materials for bearing applications. *Wear* **1995**, *184*, 45–53. [CrossRef]
14. Friedrich, K.; Reinicke, P. Friction and wear of polymer-based composites. *Mech. Compos. Mater.* **1998**, *34*, 503–514. [CrossRef]
15. Khun, N.W.; Zhang, H.; Lim, L.H.; Yue, C.Y.; Hu, X.; Yang, J. Tribological properties of short carbon fibers reinforced epoxy composites. *Friction* **2014**, *2*, 226–239. [CrossRef]
16. Ajayan, P.M.; Schadler, L.S.; Giannaris, C.; Rubio, A. Single-walled carbon nanotube-polymer composites: Strength and weakness. *Adv. Mater.* **2000**, *12*, 750–753. [CrossRef]
17. Dos Santos Barros, T.P.; De Lima Cavalcante, D.G.; De Oliveira, D.F.; Caluête, R.E.; De Lima, S.J.G. Study of the surface properties of the epoxy/quasicrystal composite. *J. Mater. Res. Technol.* **2019**, *8*, 590–598. [CrossRef]
18. Bloom, P.D.; Baikerikar, K.G.; Anderegg, J.W.; Sheares, V.V. Fabrication and wear resistance of Al–Cu–Fe quasicrystal-epoxy composite materials. *Mater. Sci. Eng. A* **2003**, *360*, 46–57. [CrossRef]
19. Sakly, A.; Kenzari, S.; Bonina, D.; Corbel, S.; Fournée, V. A novel quasicrystal-resin composite for stereolithography. *Mater. Des.* **2014**, *56*, 280–285. [CrossRef]
20. Chukov, D.I.; Stepashkin, A.A.; Tcherdyntsev, V.V.; Olifirov, L.K.; Kaloshkin, S.D. Structure and properties of composites based on polyphenylene sulfide reinforced with Al-Cu-Fe quasicrystalline particles. *J. Thermoplast. Compos. Mater.* **2018**, *31*, 882–895. [CrossRef]
21. Kenzari, S.; Bonina, D.; Dubois, J.M.; Fournée, V. Quasicrystal–polymer composites for selective laser sintering technology. *Mater. Des.* **2012**, *35*, 691–695. [CrossRef]
22. Solvay Amodel®; PPA Design Guide Amodel®. *Amodel® PPA Design Guide*; Specialty Polymers: Bollate, Italy, 2019; pp. 1–86.
23. Kušter, M.; Kovač, J.; Samardžija, Z.; Komelj, M.; Semsari Parapari, S.; Podlogar, M.; Dubois, J.-M.; Šturm, S. Impact of Tuned Oxidation on the Surface Energy of Sintered Samples Produced from Atomised B-Doped Al-Cu-Fe Quasicrystalline Powders. *Crystals* **2023**, *13*, 859. [CrossRef]
24. Vitos, L.; Ruban, A.V.; Skriver, H.L.; Kollár, J. The surface energy of metals. *Surf. Sci.* **1998**, *411*, 186–202. [CrossRef]
25. Strelniker, Y.M.; Havlin, S.; Bunde, A. Fractals and Percolation. In *Encyclopedia of Complexity and Systems Science*; Meyers, R., Ed.; Springer: New York, NY, USA, 2009; p. 10398. [CrossRef]
26. Sordelet, D.J.; Bloomer, T.A.; Kramer, M.J.; Unal, O. Effects of boron on the solidification structure of an AI-Cu-Fe alloy. *J. Mater. Sci. Lett.* **1996**, *15*, 935–939. [CrossRef]

27. *ASTM D256-10*; Standard Test Methods for Determining the Izod Pendulum Impact Resistance of Plastics. ASTM International: West Conshohocken, PA, USA, 2018.
28. Adur, A.M. Upgrading performance of recycled polyamide with ZeMac®. In *Upgrading Performance of Recycled Nylon*; Vertellus Specialties Inc.: Parsippany, NJ, USA, 2011.
29. Hutchings, I.M. *Tribology, Friction and Wear of Engineering Materials*, 1st ed.; Elsevier Limited: Oxford, UK, 1992.
30. Vollath, D. Agglomerates of nanoparticles. *Beilstein J. Nanotechnol.* **2020**, *11*, 854–857. [CrossRef]
31. Iveson, S.M.; Litster, J.D.; Ennis, B.J. Fundamental studies of granule consolidation Part 1: Effects of binder content and binder viscosity. *Powder Technol.* **1996**, *88*, 15–20. [CrossRef]
32. Anderson, W. Wettability Literature Survey—Part 2: Wettability Measurement. *J. Pet. Technol.* **1986**, *38*, 1246–1262. [CrossRef]
33. Wittmann, R.; Urban, K.; Schandl, M.; Hornbogen, E. Mechanical properties of single-quasicrystalline AlCuCoSi. *J. Mater. Res.* **1991**, *6*, 1165–1168. [CrossRef]
34. Kang, S.S.; Dubois, J.M. Compression testing of quasicrystalline materials. *Philos. Mag. A* **1992**, *66*, 151–163. [CrossRef]
35. Available online: https://www.engineersedge.com/coeffients_of_friction.htm (accessed on 1 January 2024).
36. Mihu, G.; Mihalache, I.; Graur, I.; Ungureanu, C.; Bria, V. Comparative study regarding friction coefficient for three epoxy resins. *IOP Conf. Series Mater. Sci. Eng.* **2017**, *174*, 012024. [CrossRef]
37. Durand, J.M.; Vardavoulias, M.; Jeandin, M. Role of reinforcing ceramic particles in the wear behaviour of polymer-based model composites. *Wear* **1995**, *181–183*, 833–839. [CrossRef]